Physica E 117 (2020) 113807

Contents lists available at ScienceDirect

Physica E: Low-dimensional Systems and Nanostructures

journal homepage: http://www.elsevier.com/locate/physe

Effective tuning of isotropic and anisotropic properties of quantum dots and rings by external fields

Manuk G. Barseghyan [a], Aram Manaselyan [a,*], Albert A. Kirakosyan [a], Laura M. Pérez [b], David Laroze [b]

[a] Department of Solid State Physics, Yerevan State University, Alex Manoogian 1, 0025, Yerevan, Armenia
[b] Instituto de Alta Investigación, CEDENNA, Universidad de Tarapacá, Casilla 7D, Arica, Chile

A B S T R A C T

The combined effects of intense THz laser field, magnetic field and in-plane electric field on electronic states and intraband optical properties of single isotropic quantum dots and rings are investigated using the non-perturbative Floquet theory in the high-frequency limit. Here we show that the change of the electric field direction for fixed values of intense THz laser field parameter can recover the degeneracy of the excited states and the dipole-allowed transition intensities in a quantum dot. Additionally, it is shown that in isotropic quantum rings the intense THz laser and the in-plane electric field create unusual Aharonov-Bohm oscillations. For fixed values of the intense THz laser field parameter, the amplitudes of Aharonov-Bohm oscillations can be effectively tuned by changing the electric field direction. Furthermore, for fixed values of the electric field strength and the laser field parameter the intraband optical properties can be effectively tuned by changing the electric field direction. Therefore, it can be asserted that circular quantum dots or circular rings in the intense THz laser field are equivalent to anisotropic quantum dots or rings respectively, and the electric field direction effectively tunes the single-electron energy spectrum and intraband optical properties of these structures.

1. Introduction

Modern day technologies involving nanometer-scale objects continue to improve the quality of our daily lives because the downsizing of functional units can result in a significant decrease in device energy consumption and more efficient production processes. Therefore, the fabrication and investigation of nanometer-scale systems are undoubtedly one of the central issues in current science and technology [1]. A significant class of such nanometer-scale systems are quantum dots (QDs) [2] and quantum rings (QRs) [3], which attract special attention due to their intriguing physical properties.

It is well known that in cylindrical QDs and QRs the electronic and optical properties are isotropic in the in plane directions. This isotropy of the structures can be destroyed by the nanofabrication process. It has been experimentally demonstrated [4] that tuning of the QD confinement potential offers a powerful method to manipulate the electronic states and the far-infrared intraband optical transitions in QDs. Theoretical investigation of the electronic and optical properties of anisotropic QDs in a perpendicular magnetic field and in the presence of electron-electron and Rashba spin-orbit interactions have been investigated in Refs. [5,6]. It was shown that the effect of the above-mentioned interactions on the energy spectrum and the intraband optical properties is very strong in the case of strong anisotropy of the QD. In particular, superintense and highly anisotropic optical absorption spectrum have been reported.

On the other hand, the anisotropic (spatially elliptic-shaped) QRs have been fabricated and investigated by various experimental groups [7–10]. Their results demonstrated the possibility to design and fabricate nonmagnetic QRs with magnetic properties that can be controlled by tuning the shape of the QR. Theoretically, the effect of anisotropy on electronic, magnetic, and optical properties of the QRs were investigated by various authors [11–19]. Different types of anisotropies were investigated there (shape, effective mass, defects etc.). In all cases the results have shown that the anisotropy can drastically change the electronic and optical properties of the QR.

Investigation of the magnetic field effects on the electronic and optical properties of isotropic and anisotropic zero-dimensional semiconductor nanostructures has made great progress in recent years by unraveling new phenomena and their enormous potentials in device applications [3,20]. The Aharonov-Bohm effect (AB) and the persistent current have been extensively studied in semiconductor QRs, and are expected to have potential applications in quantum electronics and quantum information. The influence of an in-plane electric field and the eccentricity on the AB effect of a semiconductor QR were investigated in

* Corresponding author.
E-mail address: amanasel@ysu.am (A. Manaselyan).

https://doi.org/10.1016/j.physe.2019.113807
Received 5 September 2019; Received in revised form 15 October 2019; Accepted 25 October 2019
Available online 31 October 2019
1386-9477/© 2019 Elsevier B.V. All rights reserved.

Refs. [21,22]. It is shown that the electric field and the eccentricity may suppress the AB oscillations of the lower energy levels. Magneto-oscillations of the electric dipole moment has been predicted and analyzed for an electron confined in an infinitely narrow QR pierced by a magnetic flux and subjected to an electric field in the ring's plane [23,24]. It is shown that these oscillations are accompanied by periodic changes in the selection rules for inter-level optical transitions in the ring, thereby allowing control of polarization properties of the associated terahertz radiation. The emission spectrum of an Aharonov-Bohm QR placed into a single-mode quantum microcavity has been investigated in Ref. [25]. It is shown that the emission spectrum in the strong coupling regime has a multiplet structure and can be tuned by the variation of the magnetic field piercing the QR and by changing the strength and direction of the applied in-plane electric field. The effects of in-plane electric field, impurity position and polarization direction on the electromagnetically induced transparency in GaAs QRs have been theoretically investigated in Ref. [26]. The electronic and optical properties of GaAs elliptic QRs under the in-plane electric field have been studied in Ref. [27]. It is shown that for both circular and non-circular QRs the intraband optical properties are very sensitive to the electric field and polarization of the probe laser.

The influence of lateral asymmetry on the electronic and optical properties in elliptical strained InAs QRs was analyzed in the presence of a perpendicular magnetic field [28]. Those studies indicate that the AB oscillations in the energy of the ground state of elongated rings disappear for a large enough magnetic field. Recently, the effect of effective mass anisotropy, ellipticity of the confinement potential and electric field on AB oscillations in QRs have been investigated in Ref. [19]. The usual AB oscillations are not observed for a circularly symmetric confinement potential. However, they can be recovered if an elliptic QR is chosen instead. The influence of anisotropy, caused by the electron-electron interaction, on AB effect in new materials, such as ZnO QRs and dot-ring structures, was reported in Refs. [29,30]. The results indicate that the AB oscillations strongly depend on the electron number in those structures.

Of late, studies of the AB effect in graphene QRs have been reported Ref. [31–33]. Most recently, the AB effect in square phosphorene QRs, with armchair and zigzag edges, has been investigated in Ref. [34]. The main result obtained in this work is that the AB oscillation, observed in the energy spectrum, strongly depends on the ring width, electric field, and the side-gating potential. Very recently, the combined influence of intense laser field (ILF) and eccentricity of QR on AB oscillations and intraband optical properties was studied in Ref. [35]. In our previous work, we have reported about theoretical investigations of ILF effect on electronic and optical properties of isotropic and anisotropic GaAs QRs in the presence of magnetic field Ref. [16]. We have shown that in isotropic QRs the laser field creates the unusual AB oscillations. In the case of anisotropic QRs we have shown that with the ILF it is possible to completely control the anisotropy of the QR and thus the physical characteristics.

In our recent work we have theoretically demonstrated the possibility of rendering of different shapes of just a single sample of a cylindrical concentric double QRs with an ILF, that in turn, allows the manipulation of electronic and optical properties of a sample [36]. Additionally, an anisotropic electronic and optical properties of isotropic concentric double QRs are modeled with the help of the ILF.

The aim of this article is to report theoretical investigations of the simultaneous influence of a THz intense laser field, lateral electric and magnetic fields on electronic states and intraband optical properties in isotropic QDs and QRs. Our work has revealed that by changing the electric field direction we can recover the isotropic properties of the anisotropic QD that were created by the ILF. It was also shown that the electric field destroys the AB oscillations in QRs even in the absence of the ILF. We have shown for the first time that the amplitude of the unusual AB oscillations can be controlled by the electric field direction. We have also shown that by changing the in-plane electric field direction and the laser field we can effectively control the intraband optical absorption in the QD and the QR. Therefore the combined influence of the in-plane electric field and the ILF can effectively tune the anisotropic properties observed in the energy and the intraband optical spectra of isotropic QDs and QRs. In the following sections, the theoretical model and the numerical methods are presented, and the results are shown and analyzed.

2. Theoretical model

Our system consists of a two-dimensional isotropic QR structure containing a single electron under the action of a homogeneous in-plane electric field and the magnetic field oriented along the growth direction. The system is radiated by the ILF which is represented by a monochromatic plane wave of frequency ν. The laser beam is non-resonant with the semiconductor structure and linearly polarized along a radial direction of the structure (chosen along the x-axis). The electron motion is described by the solution of the time-dependent Schrödinger equation:

$$\left[\frac{1}{2m}\left(\hat{\mathbf{p}}-\frac{e}{c}(\mathbf{A}(t)+\mathbf{A}_m)\right)^2+V_F(x,y)\right]\Phi(x,y,t) = i\hbar\frac{\partial}{\partial t}\Phi(x,y,t) \tag{1}$$

where m is the effective mass, $V_F(x, y) = V(x, y) - e\mathbf{Fr}$, e is the electron charge, $\hat{\mathbf{p}}$ is the lateral momentum operator of the electron, $\mathbf{A}(t) = \mathbf{e}_x A_0 \cos(2\pi\nu t)$ is the laser field vector potential, where $\mathbf{e}_x$ denotes the unit vector on the x-axis, $\mathbf{F}$ is the electric field strength. In Eq. (1), $\mathbf{A}_m$ is the vector potential of the magnetic field which is chosen to be $\mathbf{A}_m = (0, Bx, 0)$. In this case the scalar product $(\mathbf{A}(t) \cdot \mathbf{A}_m) = 0$. For the confinement potential $V(x, y)$ we choose the model of a finite, square-well type

$$V(x,y) = \begin{cases} 0, & \text{if } R_1 \le \sqrt{x^2+y^2} \le R_2, \\ V_0, & \text{otherwise,} \end{cases} \tag{2}$$

where R_1 and R_2 are the inner and outer radii of the QR, respectively. Note that, when $R_1 = 0$ our system becomes to the two-dimensional QD with radius $R_{dot} = R_2$.

Using the dipole approximation and Kramers-Hennerberger unitary transformation [37,38] in the high-frequency regime the laser-dressed energies of the QR can be obtained from the following time-independent Schrödinger equation [16,36,39–45]:

$$\left[\frac{1}{2m}\left(\hat{\mathbf{p}}-\frac{e}{c}\mathbf{A}_m\right)^2+V_d(x,y)-e\mathbf{Fr}\right]\Phi_d(x,y) = = E_d\Phi_d(x,y) \tag{3}$$

where $V_d(x, y)$ is the time-averaged laser-dressed potential that can be expressed by the following expression [16,47,48]

$$\begin{aligned} V_d(x,y) &= \frac{V_0}{\pi} Re[\pi - \\ &-\theta(\alpha_0 - x - \Gamma_1)\arccos\left(\frac{\Gamma_1 + x}{\alpha_0}\right) + \\ &+\theta(\alpha_0 - x - \Gamma_2)\arccos\left(\frac{\Gamma_2 + x}{\alpha_0}\right) - \\ &-\theta(\alpha_0 + x - \Gamma_1)\arccos\left(\frac{\Gamma_1 - x}{\alpha_0}\right) + \\ &+\theta(\alpha_0 + x - \Gamma_2)\arccos\left(\frac{\Gamma_2 - x}{\alpha_0}\right)\Big], \end{aligned} \tag{4}$$

In Eq. (4) $\Gamma_i = Re\left(\sqrt{R_i^2 - y^2}\right)$, $\theta(u)$ is the Heaviside unit-step function and $\alpha_0 = \left(e^2 I/2\pi^3 m^2 \varepsilon_h^{1/2} c\nu^4\right)^{1/2}$, which describes the strength of the laser field and comprises the intensity I, the frequency ν of the laser field,

and the high-frequency dielectric constant ε_h. Note that I and ν can be chosen for a broad range in units of kW/cm^2 and terahertz, correspondingly [43].

The laser-dressed eigenvalues E_d and eigenvectors $\psi_d(x, y)$ are found numerically, using an exact diagonalization technique. The eigenfunctions are presented as a linear expansion of the eigenfunctions of the two-dimensional rectangular infinitely high potential well with radius $R >> R_2$ [46–48]. In our calculations we have used 361 basis states which are appropriate for determining the energy eigenvalues of ground and few excited states.

We have also considered here the intraband optical transitions in the conduction band. For x-polarization of the incident light the intensity of absorption in the dipole approximation is proportional to the square of the dipole matrix element $M_{fi} \sim \langle f|x|i\rangle$, when the transition goes from the initial state $|i\rangle$ to the final state $|f\rangle$. In this work we always consider $|i\rangle$ to be the ground state.

3. Results and discussion

In this section we present the numerical simulations of our theoretical model. They are carried out for *GaAs* QD and QR with parameters $V_0 = 228$ meV, $m = 0.067m_0$ (m_0 is the free electron mass) and $\varepsilon_h = 10.9$ [49]. The radius of the QD is $R_{dot} = 20$ nm and the inner and outer radii of QR are $R_1 = 5$ nm and $R_2 = 20$ nm.

3.1. Electronic states in quantum dots

First of all let us investigate the variation of the shape of confinement potential under the action of ILF and in-plane electric field. In Fig. 1 (a) and (b) the density plots of the dressed confinement potential of the QD for two values of the ILF parameter α_0 are presented for fixed values of electric field strength (the electric field is oriented along x-direction). The ILF destroys the cylindrical symmetry of QD, and as it can be seen from both figures the shape of the QD becomes elliptically deformed. For larger values of α_0 the deviation of the confinement potential from the cylindrical symmetry is clearly visible. As a result the size quantization for low-lying states of the electron is strong, which is caused by the reduction of the effective length of the electron along the $x-$direction. In Fig. 1 (c)–(f) the density plots of the wave functions of the first three states are presented for different values of the electric field strength F_x and α_0. Note that as expected, the maximum of the ground state electron wave function is shifted from the center of the QD in the opposite direction of the electric field. Due to the presence of both fields, the cylindrical symmetry of the wave functions is destroyed as well.

Here the parity of the wave functions related to the $y-$axis (there is no defined parity for the wave functions related to the $x-$ axis): $\psi_d^{(1)}(x, -y) = \psi_d^{(1)}(x,y)$, $\psi_d^{(2)}(x,-y) = -\psi_d^{(2)}(x,y)$ and $\psi_d^{(3)}(x, -y) = \psi_d^{(3)}(x,y)$.

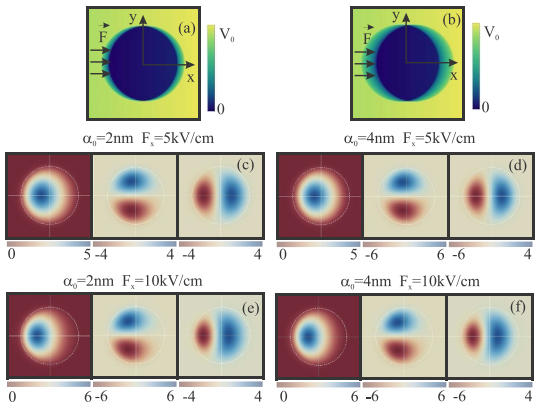


Fig. 1. (a) and (b): The density plot of the dressed confinement potential of the QD for two values of the ILF parameter $\alpha_0 = 2$ nm and $\alpha_0 = 4$ nm. The arrows indicate the direction of the electric field. (c)–(f): the density plots of the wave functions of the first three states for different values of the electric field strength F_x and α_0. The results are for $B = 0$.

In Fig. 2 (a) and (b) the density plot of the dressed confinement potential of the QD for two values of α_0 for fixed values of electric field strength are displayed when the electric field is directed along the $y-$ axis. In this case the deformation of the confinement potential under the influence of both fields is also observed. In Fig. 2 (c)–(f) the density plots of the wave functions of the first three states are presented for different values of F_y and α_0. Again, the maximum of ground state electron wave function is shifted from the center of the QD to the opposite direction of the electric field. Unlike the previous case, here the parity of the wave functions is related to the $x-$ axis (no defined parity of the wave functions related to the $y-$ axis): $\psi_d^{(1)}(-x, y) = \psi_d^{(1)}(x,y)$, $\psi_d^{(2)}(-x,y) = -\psi_d^{(2)}(x,y)$ and $\psi_d^{(3)}(-x, y) = \psi_d^{(3)}(x,y)$. An interesting effect has been observed in Fig. 2 (d) for the wave functions of the excited states. When $\alpha_0 = 4$ nm and $F_y = 5$ kV/cm the symmetry of the wave functions of the excited states is changed due to the linear Stark effect in the energy spectrum caused by the anisotropic modification of the laser-dressed confinement potential [45]. In this case, a crossing of the energy levels is observed, as a result of which the order of the energy levels and the symmetry of wave functions of first and second excited states are altered.

Fig. 3 shows the magnetic field dependence of the low-lying energy levels of an electron for various values of the electric field directed along the x-axis, and α_0. When the external ILF and the in-plane electric field are absent, we obtain the energy spectra of the cylindrical QD. These results were already reported by several authors. In this case, the energy levels of the first and second excited states at zero magnetic field are degenerate. This degeneracy disappears in the case of the shape anisotropy [5]. In our case, the ellipticity of the shape of the QD can be created by the ILF. Due to the influence of both fields, the degeneracy of the low-lying states disappear. The figures clearly show that the gap of the first and second excited states is sensitive to both fields. The energy gap of these states grows with the increase of α_0 (when the electric field strength F is fixed) and the electric field strength F (when α_0 is fixed).

Fig. 4 shows the magnetic field dependence of the low-lying energy levels of an electron for various values of the electric field directed along the y-axis, and α_0. Despite the fact that in the presence of both fields the confinement potential is anisotropic, from Fig. 4 (a) and (d) it is clearly visible that the first and second excited states are degenerate at $B = 0$ T. This is caused by the electric field: the electric field, which is directed along the y axis attempts to recover the cylindrical symmetry of the QD. The results show that the degeneracy can be recovered for $\alpha_0 = 2$ nm, $F_y = 5$ kV/cm and $\alpha_0 = 4$ nm, $F_y = 10$ kV/cm. For both cases of the electric field direction, it is notable that the crossing points of the energy levels also depend on the degree of anisotropy. This means that this value can also be controlled by the ILF parameter and the electric field

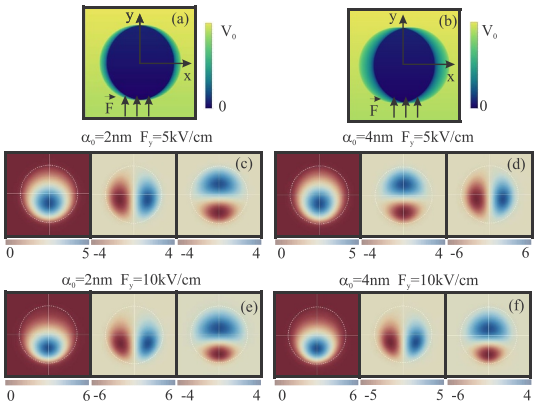


Fig. 2. Same as in Fig. 1 but the electric field is directed along the y-axis.

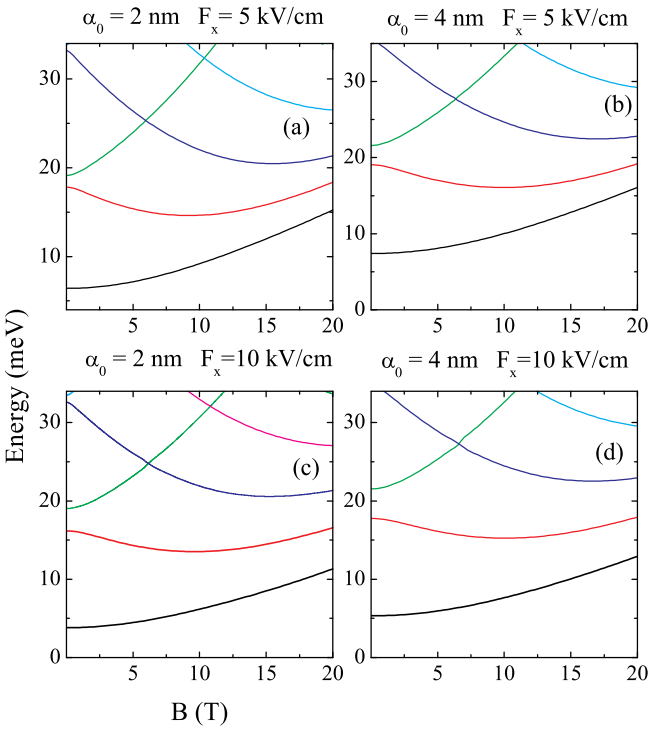


Fig. 3. Magnetic field dependence of the low-lying energy levels of an electron in the QD for different values of F_x and α_0.

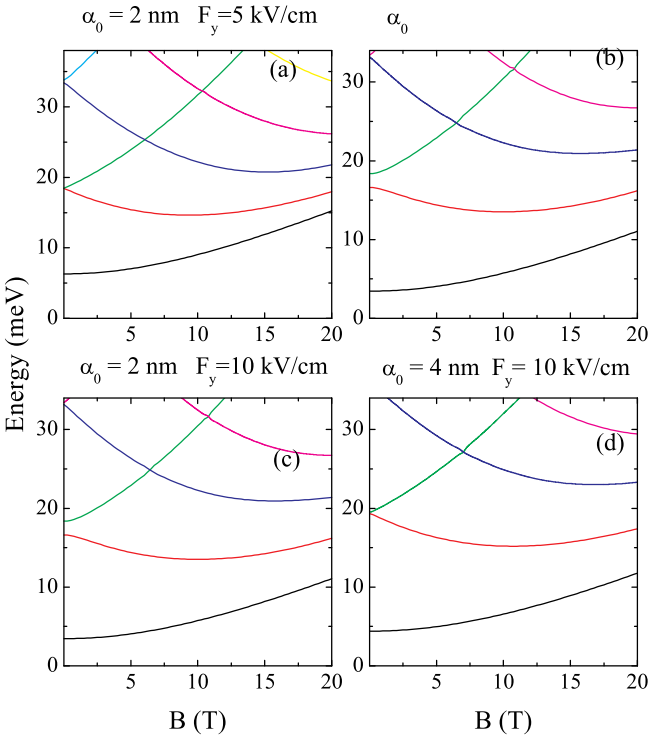


Fig. 4. Same as in Fig. 3 but the electric field is directed along the y-axis.

strength.

As we mentioned in section 2 the direction of the polarization vector $\mathbf{e}_x$ of the ILF is fixed and directed along the x axis. Considering β to be the angle between the electric field direction and $\mathbf{e}_x$, in Fig. 5 we present the electric field direction dependence of the low-lying energy levels of an electron for fixed values of the ILF parameter and the electric field

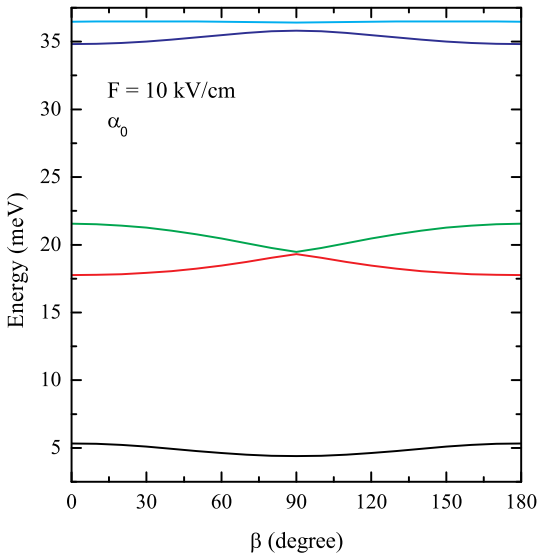


Fig. 5. Energy spectrum of a QD versus the electric field direction for $F = 10$ kV/cm, $\alpha_0 = 4$ nm and $B = 0$.

strength. It is clear that the energy levels have extrema for $\beta = 90°$. The appearance of the extrema can be attributed to the complex distribution of the electron cloud throughout the variation of β. In addition, the observed symmetry with respect to the $\beta = 90°$ point is caused by the mirror symmetry of the laser dressed confinement potential with respect to the x and y axis. This means that at angles β and $180° - \beta$ the electric field affects are the same.

3.2. Electronic states in quantum rings

In Fig. 6(a) and (b) the schematic picture of the dressed confinement potential $V_d(x, y)$ are presented for different values of the laser field intensity when the electric field is directed along the x-axis. The ILF applied on a QR creates an anisotropy in the confinement potential, and as a consequence the effective length of the confinement along the x-direction decreases in the lower part of the QR potential well. The effects of the ILF and the electric field on the corresponding ground and first two excited state wave functions are presented in Fig. 6(c)–(f). The figures reveal that the electric field always moves the wave function to the opposite direction, but the strengthening of the ILF weakens the effect of the electric field due to the enhancement of the influence of size quantization for the low-lying states.

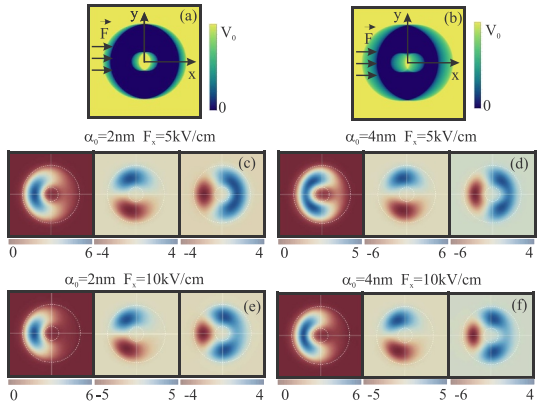


Fig. 6. (a) and (b): The density plot of the dressed confinement potential of a QR for two values of $\alpha_0 = 2$ nm and $\alpha_0 = 4$ nm. The arrows indicate the direction of the electric field. (c)–(f): The density plots of the wave functions of first three states for different values of the electric field F and α_0. The results are for $B = 0$.

In Fig. 7 (a) and (b) the schematic picture of the dressed confinement potential is presented for different values of the laser field intensity when the electric field is directed along the *y*-axis. The effects of the ILF and the electric field on the corresponding ground and first two excited state wave functions are presented in Fig. 7 (c)–(f). Analogous to the case of Fig. 2, here also we observe a symmetry change of the wave functions of the excited states in Fig. 7 (d), which again can be explained by the linear Stark effect in the energy spectrum caused by the anisotropic modification of the laser-dressed confinement potential [45].

Fig. 8 shows the magnetic field dependence of the low-lying energy levels of an electron for various values of the electric field, directed along the *x*-axis, and α_0. As was reported in our earlier work [16], the ILF creates an anisotropy in the confinement potential. Consequently, the degeneracy of the excited states for $B = 0$ disappears. With an increase of α_0 due to the reducing symmetry from C_∞ to C_2, one should expect the energy levels split into non-crossing pairs of states which in turn cross repeatedly as B increases (*unusual AB oscillations*). On the other hand, the in-plane electric field creates polar symmetry and also destroys the AB oscillations in a QR [21]. Fig. 8 represents the combined effect of the electric field and the ILF on the energy spectra and the AB oscillations of a QR. For a fixed value of α_0 with the increase of F_x, the amplitude of unusual AB oscillations decreases. Similar effects have been previously observed for phosphorene QRs in an applied electric field, directed along *x*-axis [34].

Fig. 9 shows the magnetic field dependence of low-lying energy levels for various values of the electric field, directed along the *y*-axis, and α_0. Here, the unusual AB oscillations for the combined effect of the electric field and the ILF on the energy levels are also observed. Comparing Fig. 9 (a)–(d) with Fig. 8 (a)-(d) we notice that the amplitude of the unusual AB oscillations are much bigger when the electric field is directed along the *y*-axis. It means that for fixed values of α_0 (for fixed anisotropy of the QR) the amplitude of the unusual AB oscillations can be increased by changing the direction of the electric field from the *x*-axis to the *y*-axis.

In Fig. 10 the low-lying energy levels of an electron are presented for various values of the electric field direction for fixed values of the ILF parameter and the electric field strength. The results are presented for a QR with parameters $F = 10$ kV/cm and $\alpha_0 = 4$ nm. Here one notices that the energy levels also have extrema at $\beta = 90°$. The symmetry of the energy levels in the case of a QR is observed as well. A comparison with Fig. 5 shows that in the case of a QR the energy levels are more sensitive to the angle β.

3.3. Intraband optical properties of quantum dots and quantum rings

The unusual behavior of the electron wave functions and the energy levels discussed above are expected to influence the intraband optical properties of the single QDs and QRs. In Fig. 11 the dipole-allowed optical transition energies are presented against the magnetic field for the QD with various values of the electric field F_x and α_0. The size of the circles in the figure is proportional to the intensity $|M_{fi}|^2$ of the calculated optical transitions. Due to the symmetry of the wave functions for all cases at $B = 0$ the main transition is the transition from the ground state to the second excited state ($1 \rightarrow 3$ transition). With an increase of the magnetic field the intensity of $1 \rightarrow 3$ transition decreases and the

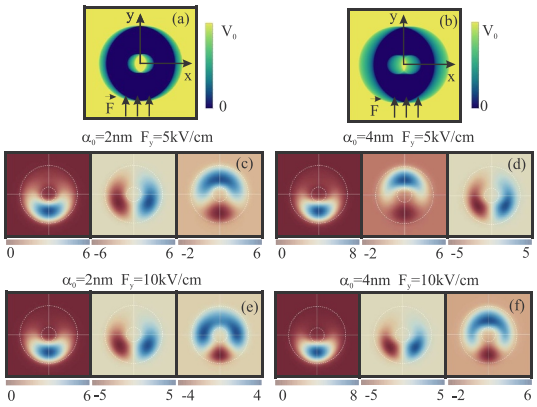


Fig. 7. Same as in Fig. 6 but the electric field is directed along the *y*-axis.

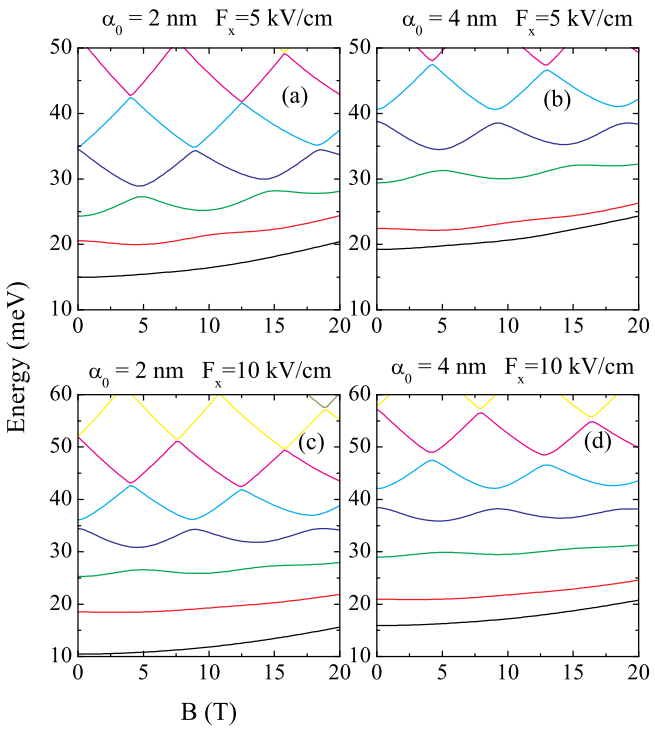


Fig. 8. Magnetic field dependence of the low-lying energy levels of an electron in a QR for different values of F_x and α_0.

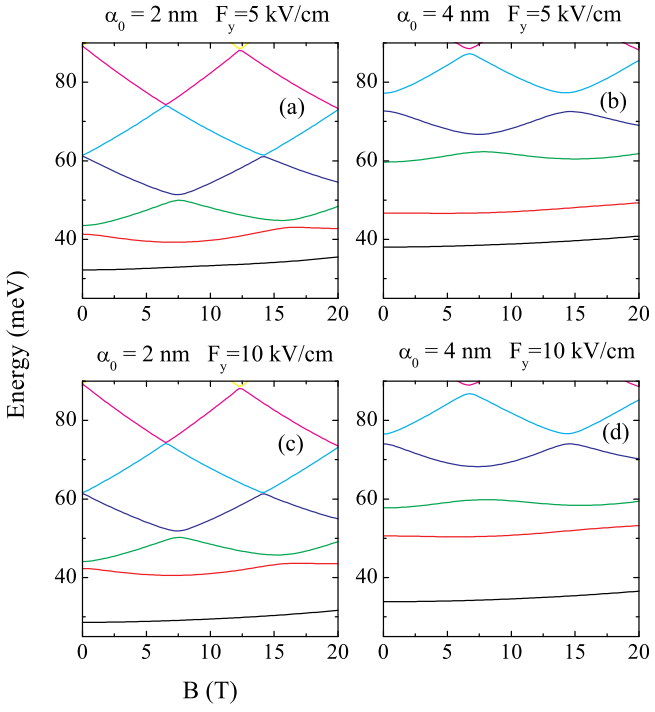


Fig. 9. Same as in Fig. 8 but the electric field is directed along the *y*-axis.

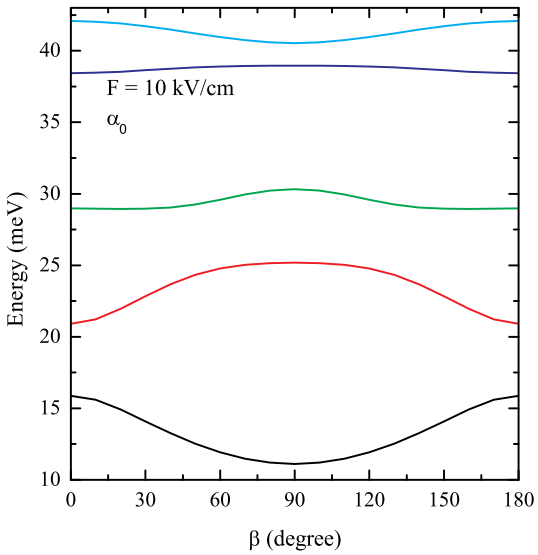


Fig. 10. The energy spectrum of a QR versus the electric field direction for $F = 10$ kV/cm, $\alpha_0 = 4$ nm, $B = 0$.

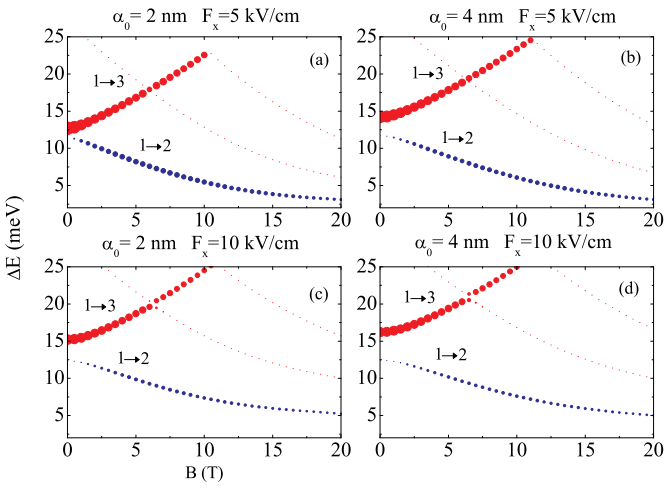


Fig. 11. The magnetic field dependence of dipole-allowed optical transition energies for different values of the electric field F_x and α_0. The size of the circles in the figure are proportional to the intensity of the calculated optical transitions. The results are for a QD.

intensity of $1 \rightarrow 2$ transition increases. Fig. 12 is similar to Fig. 11 but the electric field is directed along the y-axis. In this case at $B = 0$ the main transition is $1 \rightarrow 2$. The only exception is Fig. 12 (b), where, due to the linear Stark effect discussed above, two excited states are changed and again the main transition is $1 \rightarrow 3$.

Fig. 13 shows the dipole-allowed intraband optical transition energies as a function of the magnetic field for a QR with different values of the electric field strength and α_0, when the electric field is directed along the x-axis. The size of the circles in the figure are proportional to the intensity $|M_{fi}|^2$ of the calculated optical transitions. Here one finds that for fixed values of the electric field strength F and α_0, the unusual optical AB oscillations are observed. Note that for all these cases the intensity of the $1 \rightarrow 3$ transitions (transitions from the ground state to the second excited state) is more significant than others. This fact is caused by the symmetry of the corresponding wave functions and, as a result, by the value of corresponding dipole matrix element.

When the electric field is directed along the y-axis one can also calculate the dipole-allowed intraband optical transition energies as displayed in Fig. 14. In this case the unusual optical AB oscillations are

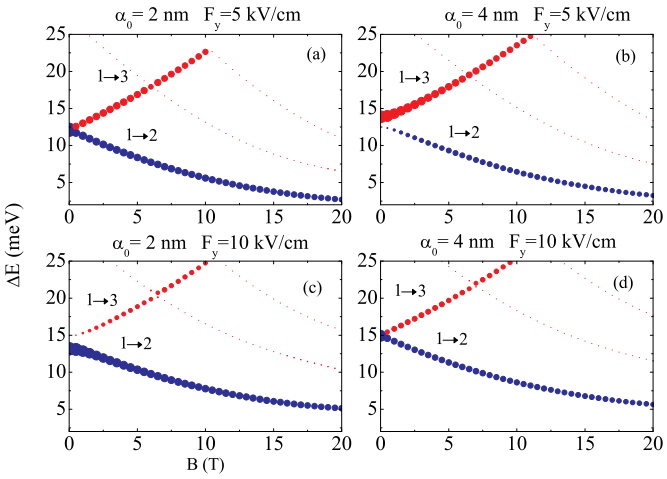


Fig. 12. Same as in Fig. 11 but for the electric field directed along the y-axis.

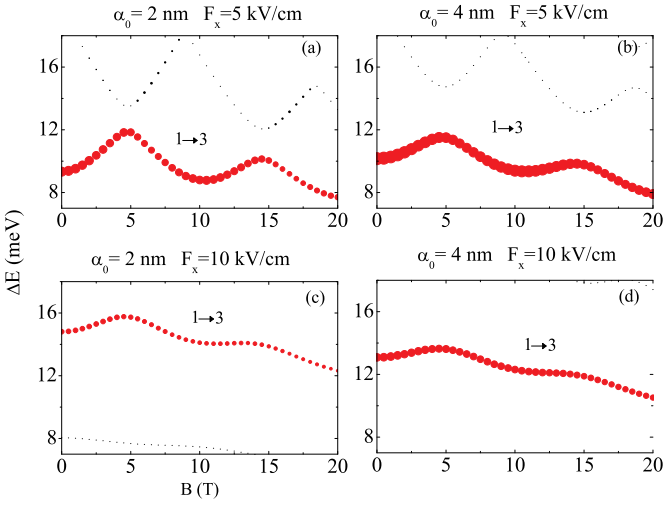


Fig. 13. The dependence of the dipole-allowed optical transition energies on the magnetic field B for different values of the electric field F_x and α_0. The size of the circles in the figures are proportional to the intensity of the calculated optical transitions. The results are for a QR.

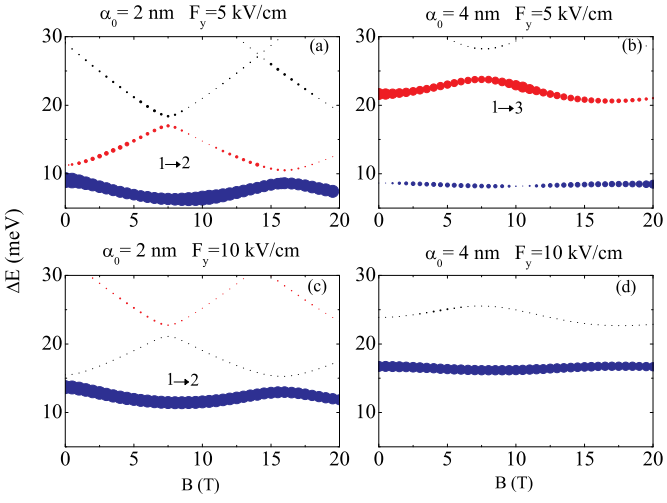


Fig. 14. Same as in Fig. 13 but for the electric field directed along the y-axis.

also visible. Except for Fig. 14(b) the intensity of the $1 \rightarrow 2$ transitions (transitions from the ground state to the first excited state) is the dominant one. When $\alpha_0 = 4$ nm and $F_y = 5$ kV/cm the symmetry of the final state wave function changes, and $1 \rightarrow 3$ transitions become much stronger.

3.4. Final remarks

We have reported here a comprehensive study of the combined influence of an intense THz laser and the in-plane electric field on the electronic and intraband optical properties of isotropic QDs and QRs in an applied magnetic field. We have shown that the change of the electric field direction for fixed values of intense THz laser field parameter can recover the degeneracy of the excited states and dipole-allowed transition intensities in a quantum dot. On the other hand, the combined action of an intense THz laser and in-plane electric field creates the unusual AB oscillations in a QR. Additionally, we have found that for fixed values of the intense THz laser field parameter, the amplitude of unusual Aharonov-Bohm oscillations can be effectively tuned by changing the electric field direction. Furthermore, we have shown that for fixed values of the electric field strength and the laser field parameter, the intraband optical properties can be drastically modified by the change of the electric field direction. Therefore it can be argued that for a fixed value of the intense THz laser field parameter, which is equivalent to the case of anisotropic quantum dot or a ring, the changing of the electric field direction effectively tunes the energy spectra and intraband optical properties of the QDs and the QRs. Finally, it is worth noting that with the change of the electric field direction, the AB oscillations in the QR can become more regular. We believe that the results are useful and will open up new avenues to improve the design and characterization of future novel devices based on single QDs and QRs, such as THz detectors, efficient solar cells as well as the photon emitters.

Declaration of competing interest

All the authors declare that they do not have any conflicts of interests.

Acknowledgments

All authors thank professor Tapash Chakraborty for helpful discussions and useful advises. MGB and AM acknowledge the financial support by the Armenian State Committee of Science (Project no. 18T-1C223). LMP and DL acknowledge partial financial support from FONDECYT 1180905. DL acknowledges partial financial support from Centers of excellence with BASAL/CONICYT financing, Grant FB0807, CEDENNA.

References

[1] A.P. Alivisatos, Science 271 (1996) 933.
[2] T. Chakraborty, Quantum Dots, Elsevier, Amsterdam, 1999.
[3] V.M. Fomin (Ed.), Physics of Quantum Rings, Springer-Verlag, Berlin, 2018.
[4] A. Singha, V. Pellegrini, S. Kalliakos, B. Karmakar, A. Pinczuk, L.N. Pfeiffer, K. W. West, Appl. Phys. Lett. 94 (2009), 073114.
[5] A.V. Madhav, T. Chakraborty, Phys. Rev. B 49 (1994) 8163.
[6] S. Avetisyan, P. Pietiläinen, T. Chakraborty, Phys. Rev. B 88 (2013), 205310.
[7] R. Blossey, A. Lorke, Phys. Rev. E 65 (2002), 021603.
[8] P. Offermans, P.M. Koenraad, J.H. Wolter, D. Granados, J.M. Garcia, V.M. Fomin, V.N. Gladilin, J.T. Devreese, Appl. Phys. Lett. 87 (2005), 131902.
[9] N.A.J.M. Kleemans, I.M.A. Bominaar-Silkens, V.M. Fomin, V.N. Gladilin, D. Granados, A.G. Taboada, J.M. García, P. Offermans, U. Zeitler, P.C. M. Christianen, J.C. Maan, J.T. Devreese, P.M. Koenraad, Phys. Rev. Lett. 99 (2007), 146808.
[10] J. Wu, Z.M. Wang, K. Holmes, E. Marega Jr., Z. Zhou, H. Li, Y.I. Mazur, G. J. Salamo, Appl. Phys. Lett. 100 (2012), 203117.
[11] V.M. Fomin, V.N. Gladilin, S.N. Klimin, J.T. Devreese, N.A.J.M. Kleemans, P. M. Koenraad, Phys. Rev. B 76 (2007), 235320.
[12] J. Planeles, F. Rajadell, J.I. Climente, Nanotechnology 18 (2007), 375402.
[13] G.A. Farias, M.H. Degani, J.A.K. Freire, J. Costa e Silva, R. Ferreira, Phys. Rev. B 77 (2008), 085316.
[14] L. Wendler, V.M. Fomin, A.A. Krokhin, Phys. Rev. B 50 (1994) 4642.
[15] L. Wendler, V.M. Fomin, Phys. Status Solidi B 191 (1995) 409.
[16] T. Chakraborty, A. Manaselyan, M. Barseghyan, D. Laroze, Phys. Rev. B 97 (2018), 041304(R).
[17] J.A. Vinasco, A. Radu, E. Kasapoglu, R.L. Restrepo, A.L. Morales, E. Feddi, M. E. Mora-Ramos, C.A. Duque, Sci. Rep. 8 (2018) 13299.
[18] A. Ghazaryan, A. Manaselyan, T. Chakraborty, Phys. Rev. B 93 (2016), 245108.
[19] G.O. de Sousa, D.R. da Costa, A. Chaves, G.A. Farias, F.M. Peeters, Phys. Rev. B 95 (2017), 205414.
[20] D. Heitmann (Ed.), Quantum Materials, Springer-Verlag, Heidelberg, 2010.
[21] Z. Barticevic, G. Fuster, M. Pacheco, Phys. Rev. B 65 (2002), 193307.
[22] A. Bruno-Alfonso, A. Latgé, Phys. Rev. B 71 (2005), 125312.
[23] A.M. Alexeev, M.E. Portnoi, Phys. Rev. B 85 (2012), 245419.
[24] A.M. Alexeev, M.E. Portnoi, Phys. Status Solidi C 9 (2012) 1309.
[25] A.M. Alexeev, I.A. Shelykh, M.E. Portnoi, Phys. Rev. B 88 (2013), 085429.
[26] D. Bejan, C. Stan, E.C. Niculescu, Opt. Mater. 75 (2018) 827.
[27] D. Bejan, C. Stan, E.C. Niculescu, Opt. Mater. 78 (2018) 207.
[28] M.M. Milošević, M. Tadić, F.M. Peeters, Nanotechnology 19 (2008), 455401.
[29] T. Chakraborty, A. Manaselyan, M. Barseghyan, J. Phys. Condens. Matter 29 (2017), 215301.
[30] T. Chakraborty, A. Manaselyan, M. Barseghyan, Physica E 99 (2018) 63.
[31] D.S.L. Abergel, V.M. Apalkov, T. Chakraborty, Phys. Rev. B 78 (2008), 193405.
[32] M. Zarenia, J.M. Pereira, A. Chaves, F.M. Peeters, G.A. Farias, Phys. Rev. B 81 (2010), 045431.
[33] I. Romanovsky, C. Yannouleas, U. Landman, Phys. Rev. B 85 (2012), 165434.
[34] L.L. Li, D. Moldovan, P. Vasilopoulos, F.M. Peeters, Phys. Rev. B 95 (2017), 205426.
[35] J.A. Vinasco, A. Radu, E. Niculescu, M.E. Mora-Ramos, E. Feddi, V. Tulupenko, R. L. Restrepo, E. Kasapoglu, A.L. Morales, C.A. Duque, Sci. Rep. 9 (2019) 1427.
[36] H.M. Baghramyan, M.G. Barseghyan, A.A. Kirakosyan, J.H. Ojeda, J. Bragard, D. Laroze, Sci. Rep. 8 (2018) 6145.
[37] H.A. Kramers, Collected Scientific Papers, North-Holland, 1956.
[38] W.C. Henneberger, Phys. Rev. Lett. 21 (1968) 838.
[39] M. Gavrila, J.Z. Kaminski, Phys. Rev. Lett. 52 (1984) 613.
[40] M. Pont, N.R. Walet, M. Gavrila, C.W. McCurdy, Phys. Rev. Lett. 61 (1988) 939.
[41] E.C. Valadares, Phys. Rev. B(R) 41 (1990) 1282.
[42] M. Gavrila, J. Phys. B At. Mol. Opt. Phys. 35 (2002) R147.
[43] S.D. Ganichev, W. Prettl (Eds.), Intense Terahertz Excitation of Semiconductors. Semiconductor Science and Technology, Oxford University Press, Oxford, 2006.
[44] U. Yesilgul, E.B. Al, J.C. Martínez-Orozco, R.L. Restrepo, M.E. Mora-Ramos, C. A. Duque, F. Ungan, E. Kasapoglu, Opt. Mater. 58 (2016) 107.
[45] H.M. Baghramyan, M.G. Barseghyan, D. Laroze, Sci. Rep. 7 (2017) 10485.
[46] S. Gangopadhyay, B.R. Nag, Nanotechnology 8 (1997) 14.
[47] A. Radu, A.A. Kirakosyan, D. Laroze, H.M. Baghramyan, M.G. Barseghyan, J. Appl. Phys. 116 (2014), 093101.
[48] A. Radu, A.A. Kirakosyan, D. Laroze, M.G. Barseghyan, Semicond. Sci. Technol. 30 (2015), 045006.
[49] S. Adachi, Handbook on Physical Properties of Semiconductors, vol. 2, Kluwer Academic Publishers, New York, 2004.